Materials Science & Engineering A 857 (2022) 144097

Contents lists available at ScienceDirect

Materials Science & Engineering A

journal homepage: www.elsevier.com/locate/msea

In-situ analysis of the elastic-plastic characteristics of high strength dual-phase steel

Simon Vitzthum [a,*], Joana Rebelo Kornmeier [b], Michael Hofmann [b], Maximilian Gruber [a], Roman Norz [a], Emad Maawad [c], Joseba Mendiguren [d], Wolfram Volk [a]

[a] Chair of Metal Forming and Casting, Technical University of Munich, Garching Near, Munich, Germany
[b] Heinz Maier-Leibnitz Zentrum (MLZ), Technical University of Munich, Garching Near, Munich, Germany
[c] Helmholtz-Zentrum Hereon, Institute of Materials Physics, Geesthacht, Germany
[d] Mondragon Unibertsitatea, Faculty of Engineering, Mechanics and Industrial Production, Mondragon, Gipuzkoa, Spain

ARTICLE INFO

Keywords:
High-strength steel
Elastic-plastic material behavior
In-situ diffraction
Evaluation approach

ABSTRACT

Modeling the elastic behavior of dual-phase steels is complex due to the strain dependency of Young's modulus and high elastic nonlinearity. Since it is assumed that reasons for this are to be found in microstructural behavior, microscopic in-situ analysis are necessary, but due to the overlap of the martensite and ferrite peaks, the evaluation of diffraction profiles is highly complex. Within this work, CR590Y980T (DP1000) is investigated in a continuous cyclic tensile and tension-compression test under synchrotron radiation at High Energy Material Science beamline P07 in Petra III, DESY. On basis of additional EBSD measurements, an evaluation approach is shown to analyze the dual-phase diffraction profiles in such a way that martensite and ferrite can be separated for three lattice planes. The origin of the specific elastic-plastic behavior of dual-phase steels in terms of onset of yielding, anelasticity or early re-yielding is analyzed on the basis of lattice strains and interphase stresses. For this, the time-synchronously measured micro data is correlated with the macro stress-strain relationship and thermoelastic effect. The results help to better understand strain-dependent elastic-plastic behavior of DP steels on a micro level and provide great potential to improve characterization and modeling in terms of springback prediction.

1. Introduction

Accurate springback prediction is still one of the big challenges and, accordingly, an ongoing field of research in metal forming. Both experimental methods and numerical modeling have improved significantly in recent years [1]. Precise material models with respect to the elastic-plastic behavior of materials are the basis for accurate FE simulation [2]. However, the elastic-plastic behavior of steels in general and of dual-phase steel grades particularly pose challenges. These challenges in modeling elastic material behavior can be summarized as follows:

- Determination of the initial Young's modulus and the onset of plastic yielding in case of a steady elastic-plastic transition
- Strain-dependent, nonlinear elastic, i.e. anelastic, behavior
- Early re-yielding or strongly pronounced Bauschinger effect

Due to the high strength respectively hardening of the dual-phase steels, they exhibit a particularly large elastic range, which is why the properties mentioned above have an even greater effect with regard to springback [3]. In material science, it has long been known that elastic material behavior deviates from the idealized linear behavior [4], also known as Hooke's law [5]. The determination of the yield strength and Young's modulus is a key factor for springback prediction [3]. A large number of materials show a steady elastic-plastic transition and differ significantly in their stress-strain behavior. Accordingly, a clear determination of the lower and upper limits for the evaluation of the initial slope of the yield curve is often not possible [6]. In several studies [7,8] approaches for the determination of the Young's modulus as well as the onset of yielding [9] are shown, but none of these is physically based and depending on the determination method, large deviations can occur [10]. Vitzthum et al. [11] introduced a temperature-dependent determination method and recently verified it by an in-situ study for a single-phase steel [12]. The study shows the relation between the onset of yielding and the thermoelastic effect on a micro level and

* Corresponding author.
E-mail address: simon.vitzthum@tum.de (S. Vitzthum).

https://doi.org/10.1016/j.msea.2022.144097
Received 23 August 2022; Received in revised form 22 September 2022; Accepted 24 September 2022
Available online 30 September 2022

temperature-based determination methods for both the onset of yielding and the elastic loading modulus. Within the current study, their applicability will be shown also for dual-phase materials on a micro level.

The plastic strain-dependency of the elastic behavior was already noticed by Taylor and Quinney in the beginning of the 20th century [13]. It is well known that considering the change of the elastic modulus and the Bauschinger effect as a function of plastic strain is crucial for springback prediction and cannot be neglected [14]. To determine an unloading modulus, mostly the chord modulus (E_{chord}) is used, which is the linear connection between the start of unloading and the stress-free point at complete unloading (0 MPa) [3]. Some linear modeling approaches describe this reduction of the chord modulus mathematically [15–17]. Yoshida and Uemori [18] introduced a widely-used one and subsequently extended it to include nonlinearity [19].

Starting from Zener and Hollomon [20], numerous different definitions for anelasticity can be found in the literature. In this work, the approach of Li and Wagoner [4] is followed, who equated anelasticity to nonlinear elasticity in their extensive study. This means that the reduction of the chord modulus respectively the nonlinear behavior is related to a recovery or springback strain ($\varepsilon_{\text{springback}}$) that exceeds the linear expected strain recovery ($\varepsilon_{\text{elastic}}$). This additional strain is called anelasticity, or anelastic strain ($\varepsilon_{\text{anelastic}}$) (see Fig. 1) [21]. Mathematically this relation can be described as follows [22].

$$\varepsilon_{\text{springback}} = \varepsilon_{\text{anelastic}} + \varepsilon_{\text{elastic}} = \varepsilon_{\text{anelastic}} + \frac{\sigma}{E_0} \tag{1}$$

There, E_0 is the initial Young's modulus and σ the current true stress or Cauchy stress. Li and Wagoner [4], based on new findings, defined the anelastic behavior as energy consuming like plastic strain and reversible like elastic strain. Several explanation approaches for this special material behavior can be found in the literature [23]. In extensive studies, dislocation motion and microstructural interphase stresses have been found to be the most plausible as responsible mechanisms [24]. Cleveland and Ghosh [16] explain the anelastic behavior with mobile dislocations, which pile-up at grain boundaries in forward direction (loading). Backwards (unloading), first the piled-up dislocation retreat, before also cell wall dislocations start to move reversely. With decreasing stress more and more piled-up mobile dislocations move. This leads to the additional anelastic strain, or nonlinearity. Several studies support this assumption and a summary can be found in Li and Wagoner's work [4]. In Govik et al. [25], it is shown by means of a simulation model that the strongly different behavior of the martensite (Ma) and ferrite (Fe) phases lead to interphase stresses. These stresses within grains can be responsible for the nonlinear behavior even below yielding. Zecevic et al. [26] also investigated the behavior of a DP590 steel using an enhancement of a crystal plasticity model and was able to work out influences on the elastic-plastic behavior of a dual-phase steel in simulations. In addition to model parameters, the effect of nihilation of dislocations and plastically deformable martensite was investigated. The model was calibrated based on existing model approaches in literature and estimates. Both explanations for anelastic behavior, dislocation motion and interphase stresses, involve processes in the microstructure of the material. Accordingly, microscopic investigations are necessary to verify existing assumptions. There are studies, which show microstructural results for dual-phase steels on basis of ex-situ microscopy methods like EBSD measurements [27].

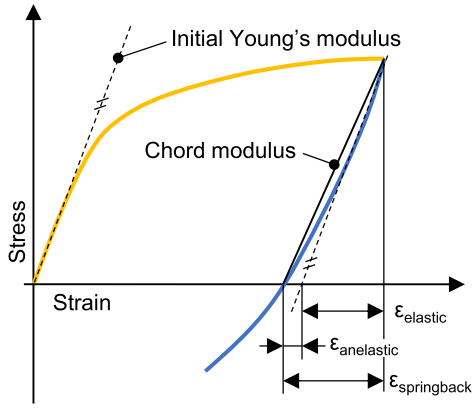

Fig. 1. Schematic stress-strain curve to illustrate the elastic material behavior and its parameters.

For an even more precise investigation of the elastic material behavior, in-situ experiments are necessary that allow an analysis of the microstructural behavior under stress in a continuous test. Over time, in-situ diffraction experiments have evolved and high-energy X-ray diffraction experiments with single-phase materials are often found in the field of material characterization [28–30]. The high formability combined with high strength is based on the special microstructure of DP steels. It is composed of a soft ferritic and a hard martensitic phase [31]. More understanding for the micromechanical behavior of these phases during plastic deformation can lead to higher accuracy in numerical simulation models [32]. However, the evaluation of in-situ diffraction tests with martensitic-ferritic steels is not trivial because of the strong overlap between the two phases due to the very similar crystal structure [33]. The separate evaluation of the two phases, though, has already been demonstrated with neutrons [32] and high-energy X-ray diffraction [34].

In the state of the art, mainly standard tensile tests have been investigated by in-situ diffraction experiments to calibrate and validate crystal models. Most of these tests are not continuous, which can lead to errors due to relaxation effects. Cyclic tensile tests are necessary for the in-situ investigation of the elastic nonlinearity as a function of plastic strain. In order to be able to investigate the unloading behavior in detail, a high resolution and measuring frequency is important for the recorded diffraction profiles.

In this study, high-energy synchrotron transmission measurements are performed in the German Electron Synchrotron (DESY). The considered dual-phase steel (CR590T980Y) is tested in a continuous, cyclic tensile test and diffraction measurements are performed with a high frequency (1 Hz) for this kind of measurement. Furthermore, the specimen temperature is measured during the test to analyze and determine the loading modulus and onset of plastic yielding by means of the thermoelastic effect [12]. Based on EBSD results on the phase fractions, the peak shifts of the diffraction profiles and thus the lattice strains of the martensite and ferrite are evaluated separately for the lattice planes (110), (200) and (211). The nonlinear macroscopic behavior is analyzed by phase-dependent evaluation of lattice strains and phase stresses. For the investigation of the possible early re-yielding, or the Bauschinger effect, a continuous tension-compression test is performed to investigate the microstructural behavior not only for the unloading but also for compression. In this way, lattice strains are used to show when the individual lattice planes begin to re-yield after load change. The study provides extensive results on the relationship of interphase stresses with plastic strain-dependent elastic material behavior. The measurement method used allows a relative comparison of the microstructural material behavior to the initial state as a function of plastic strain. These results are of great importance in particular for a better understanding of the springback behavior. The course of residual stresses of a dual-phase material over the forming process can thus be demonstrated, even if the initial state after sheet production cannot be quantified in more detail with this measurement technology. Based on the latest experimental technology, material understanding is increased and material characterization is improved. The study uses the nomenclature listed in Table 1.

2. Material

The dual-phase, high strength steel CR590Y980T (DP1000) is

Table 1
Nomenclature used within this work.

Name	Unit	Definition
True stress	[MPa]	Macroscopic Cauchy stress
True strain	[−]	Macroscopic Hencky strain
Relative temperature	[K]	Specimen temperature relative to the initial temperature at experiment start
Intensity	[−]	Counts for diffraction reflex
Lattice strain	[µm/m]	Lattice plane specific lattice strain, dependent on the shift of the center position of the reflex
Phase stress	[MPa]	Phase dependent stress of specific lattice plane determined by the corresponding DEC_{hkl}

considered with a sheet thickness of 1.5 mm. DP1000 is a ferritic-martensitic steel and is suitable for lightweight construction due to its beneficial high strength-mass relationship. This composition of the two phases is produced by a special heat treatment of a low carbon steel. The material under study, having a yield strength of ~698 MPa at 0.2% plastic strain and a tensile strength of ~1047 MPa, is often used for crash-relevant parts in the vehicle body, such as the pillars [35]. Fig. 2 (a) shows the materials microstructure acquired with a Scanning Electron Microscope (SEM). As can be seen, this material is a fine-grained material with an average grain size around 2 µm [36]. Table 2 shows the chemical composition determined by Optical Emission Spectrometer (OES). For the conducted cyclic tensile tests, the specimen geometry according to the standard (DIN EN ISO 50152, Form H [37]) was used with a parallel length of 75 mm, a width of 12.5 mm and 50 mm gauge length (see Fig. 2 (b)). In this study, only tensile tests in rolling direction were performed.

3. Experimental setup and procedure

The in-situ diffraction experiments were conducted at the High Energy Materials Science beamline HEMS, P07B, of Helmholtz-Zentrum Hereon at PETRA III (DESY, Hamburg). In the following, the most important settings for the investigations within this study are discussed. More details about the experimental setup can be found in Vitzthum et al. [12]. A single bounce monochromator (SBM) with a flat water-cooled Laue crystal Si (220) was used to monochromatize the high-energy X-ray beam. With this setting, a wavelength of 0.14235 Å was achieved. The beam size was 0.7 × 0.7 mm^2. The PerkinElmer XRD 1621 flat panel with a resolution of 2048 × 2048 pixels (200 × 200 $µm^2$ pixel size), was adjusted to a specimen to detector distance of 1606.2 mm, so that three complete Debye-Scherrer rings could be obtained (see Fig. 3). The detector settings were calibrated and misalignments corrected by Lanthanhexaborid (LaB6) powder measurements, which were evaluated using the software Fit2D [38]. The frequency was set to one diffraction measurement per second. Fig. 4 shows the basic experimental setup schematically.

Cyclic tensile tests were performed with four unloading-loading cycles distributed over a true plastic strain of 6 % (see Fig. 5 (a)). The fast data acquisition of the synchrotron measurement made it possible to conduct continuous tensile tests without measurement stops and still have high resolution. The specimen was mounted in a self-developed tensile test machine [39] and clamped in specially developed horizontal clamping specimen grips (see Fig. 6 (a)). The crosshead speed was set to 0.9 mm/min displacement controlled, which resulted in a strain rate of about $1.5 \bullet 10^{-4}$ s^{-1} based on the strain measured by the strain gage. The macroscopic load was measured by a load cell, the strain by a strain gage and the specimen temperature by a PT1000 sensor (see details in [12]). All data were acquired time-synchronously in a measurement system and synchronized with the microscopic data via a start trigger. The tension-compression test was carried out using the same measuring technique and test settings. The specimen was first elongated to 3 % true strain and then compressed to - 0.4% true strain. To prevent buckling under compressive stress, a buckling support in the form of interlocking teeth, based on the test settings used in Kuwabara et al. [40], was additionally mounted on the specimen grips (see Fig. 6 (b)). A measuring window with an area of 18 × 6 mm^2 in starting position for the strain gage and the synchrotron beam is located in the center of the buckling support so that the measurement is not influenced by the buckling support. No specimen temperature could be measured due to the limited space for measurement sensors in the measurement window. Fig. 5 (b) shows the macroscopic true stress versus true strain curve of the tension-compression experiment.

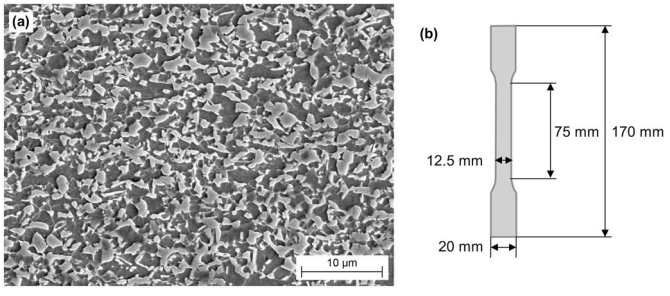

Fig. 2. (a) Microstructure of ferritic-martensitic DP1000 (SEM image); (b) Specimen geometry for both tensile and tension-compression tests.

4. Evaluation approach for dual phase steel

4.1. Determination of phase fractions

Peak intensities, measured by in-situ experiments, are proportional to the phase fractions in multiphase materials [41]. That is why, the phase fractions of the martensite and ferrite were determined as a boundary condition for fitting the overlapping peaks. For this purpose, Scanning Electron Microscope (SEM) images were taken and a gray-scale value analysis was performed to distinguish between the phases. The SEM images of all the specimens were taken using rolling direction-transverse direction (RD-ND and TD-ND) planes. The measured surface was prepared using mechanical grinding with up to P1200 sandpaper, followed by mechanical polishing in 6 µm, 3 µm and 1 µm diamond suspension. The final preparation was 2 h in a VibroMet™ 2 vibratory polisher using colloidal silica suspension. All SEM analyses were conducted at 30 kV acceleration voltage and a working distance of 7 mm with a 70° tilting angle. Regions with an area of 170 µm × 120 µm and a step size of 0.16 µm with a exposure time of 4.02 ms, were measured for each specimen. The data was summarized for both local and statistical microstructure characterization. The Matlab MTEX toolbox [42] was employed to analyze the grain and sub-grain microstructure. Fig. 7 (a) shows the SEM image for the considered material. The lighter shades of gray, or the areas that appear highlighted, are the embedded martensite phase. The darker, larger-area zones represent the ferrite phase. In DP materials, there is a grain boundary layer between the phases, and there may also be retained austenite. In the case of DP1000 with high martensite content, however, this boundary layer is hardly present and was therefore not taken into account. No retained austenite could be detected in the diffraction profiles, which is why austenite was also not taken into account in the evaluation. The gray values were identified and divided into white and black fractions with a Matlab script (see Fig. 7 (b)). Afterwards, the white and black pixels were counted and thus the ratio between martensite and ferrite could be determined. Five images at five different locations were used and an average composition of 36 % martensite and 64 % ferrite was obtained, which is in good agreement with the results in Woo et al. [32], who investigated a very similar dual-phase steel.

4.2. Peak profile analysis

Debye-Scherrer rings were recorded and integrated for specific

Table 2
Chemical composition in [%] – mass fraction.

	C	Si	Mn	P	S	Al	Ti	Nb	Cr	Mo	V	B
DP1000	0.12	0.20	2.00	0.02	0.01	0.18	0.05	0.02	0.35	0.05	0.01	0.01

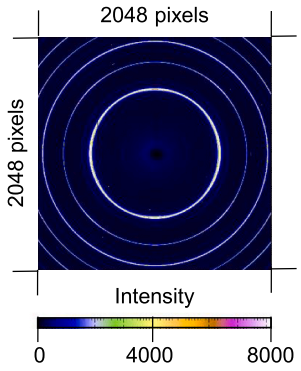

Fig. 3. Debye-Scherrer rings for DP1000, obtained by in-situ diffraction experiments.

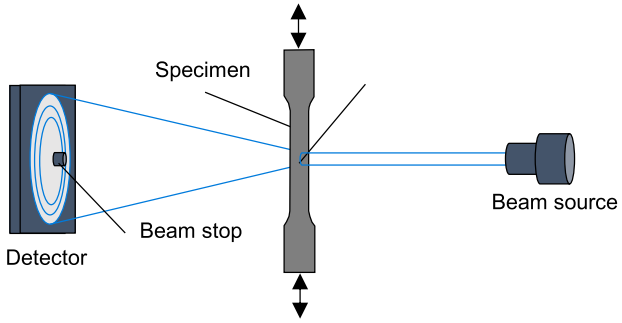

Fig. 4. Basic experimental setup and macroscopic test procedure for in-situ, cyclic tensile and tension-compression tests.

sectors using Fit2D software [38], as already described in detail in Vitzthum et al. [12]. The intensities of the sectors were summed in longitudinal direction to get better statistics for the evaluation of the two overlapping peaks, (see Fig. 8). With the chosen settings, it was possible to evaluate the lattice planes (110), (200), and (211).

For the peak fitting, the Matlab-based Line-Profile Analysis Software (LIPRAS) was used [43]. This allowed the fitting of overlapping reflections. In addition, several fit functions are available and boundary conditions for the intensity values, full width at half maximum (FWHM) and center positions can be set. It is already known from studies that the distinction between the martensite and ferrite peak is clearer at higher pre-strains [44]. For this reason, the diffraction profiles were evaluated in the inverse direction, starting from high plastic strain to initial state. As a boundary condition the intensities of the reflections of each phase were constrained for each lattice plane to have the same ratio as the phase proportions measured by SEM and that their sum is in good agreement with the experimental points. No other limits were assigned to the ferrite phase. It was assumed that the FWHM of the respective phase is lowest in the initial state and increases with increasing plastic strain. On this basis, the minimum value of the FWHM of the martensite peak was adjusted to give low errors for the fitting results, especially in the foot region of the overall peak in the initial state. Fig. 9 shows the diffraction profiles of the (211) lattice plane for the initial state at 0 % true plastic strain (ε_{pl}) (a), after the second unloading at 1.85 % true

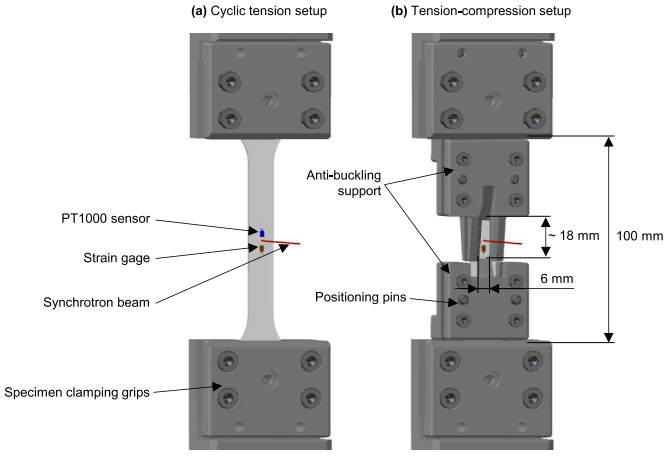

Fig. 6. View of the experimental setups with measurement sensors and synchrotron beam for (a) the cyclic tensile tests and (b) the tension-compression tests.

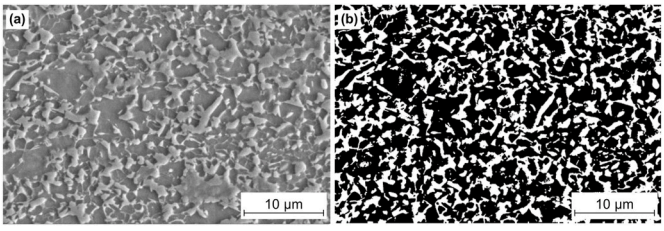

Fig. 7. SEM image (a) and corresponding black and white image (b) after gray-scale value analysis to determine the phase fractions.

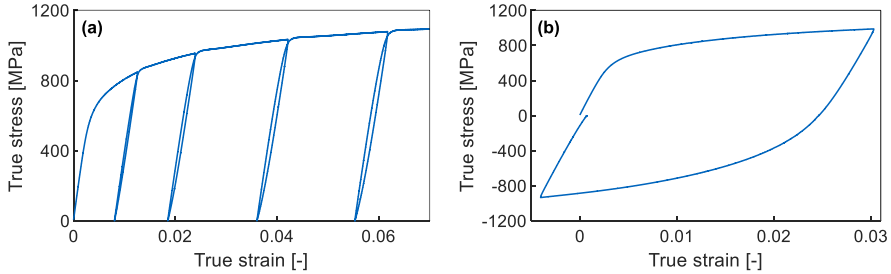

Fig. 5. Macroscopic true stress – true strain curve for (a) cyclic tensile test and (b) tension-compression test.

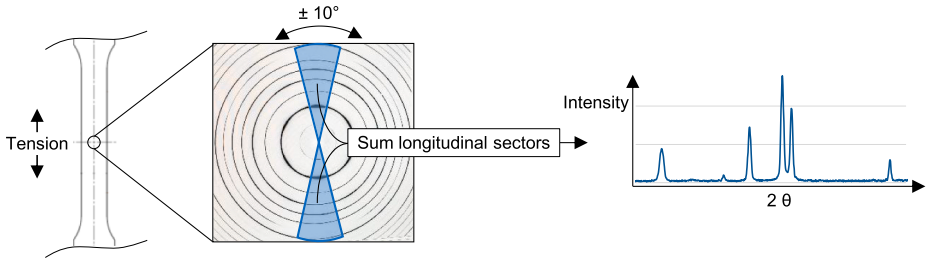

Fig. 8. Schematic representation of the procedure for evaluating Debye-Scherrer rings.

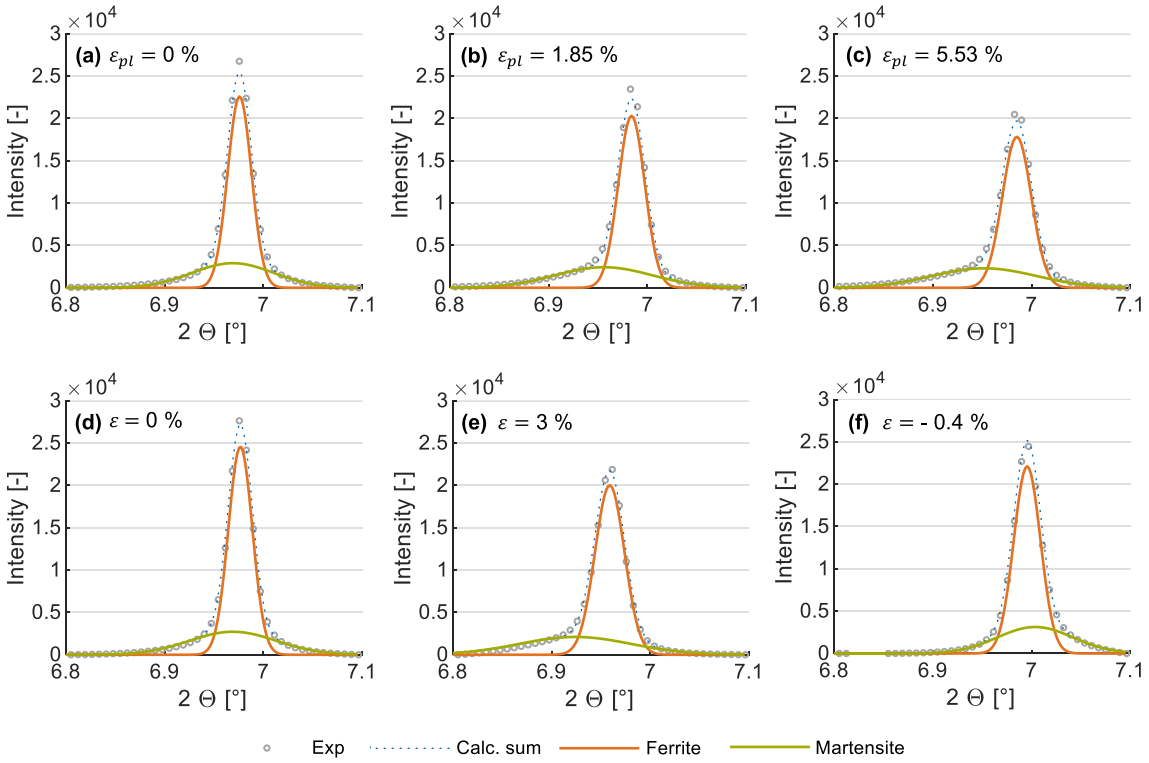

Fig. 9. Experimentally measured intensities (counts) versus 2 Θ range with Gauss fits for the martensite and ferrite peaks with their calculated sum curve. Plots represent the diffraction peaks for the (211) lattice plane for different states during the cyclic tensile test (a–c) and tension-compression test (d–f).

plastic strain (b) and after the fourth unloading at 5.53 % true plastic strain (c). Shown are the states without external load, so at zero true stress (0 MPa). In addition, the initial state (d), the state at 3 % true strain (ε) (e), and the state after subsequent compression loading at - 0.4 % true strain (f) of the tension-compression test are shown. Since within this study mainly processes based on micro strains were to be investigated, the Gaussian function was used for peak profile analysis [45]. It can be seen, as mentioned earlier, that at the initial state, it is difficult to distinguish between the two phases, as they overlap completely in the material present (see Fig. 9 (a) and (d)). The foot of the overall measured peak is clearly different from a Gaussian fit. Thus, the foot must come from the wider martensite peak with lower maximum intensity. However, after the fourth unloading at more than 5 % true plastic strain (see Fig. 9 (c)), a clear shift of the reflections of the phases to each other can be appreciated. It can be seen that the experimental reflection got significantly wider with increasing plastic strain. Since no phase transformations take place in this material, the shape area of the peaks remains the same, so the intensity must decrease with increasing plastic strain. Fig. 9 (a)–(c) show this behavior clearly. The diffraction profile after subsequent compressive loading is highly interesting (see Fig. 9 (f)). On the one hand, it shows that the martensite peak moves to higher 2θ angles compared to the ferrite peak and is thus on the other side in the foot of the experimental data. On the other hand, it can be seen that the peak widths become narrower again and that the peak height also increases again due to the greater overlap.

In this study, the interphase stresses are analyzed based on the separate evaluation of the lattice strains of the martensite and ferrite phases (ph) and their diffraction elastic constants (DEC_{hkl}). The phase specific lattice strains ε^{ph}_{hkl} were determined by calculating the atomic distance d^{ph}_{hkl} with the respective 2θ center position via Bragg's Law [46] and relating it to the initially measured atomic distance $d^{ph,0}_{hkl}$ as follows [47,48].

$$\varepsilon^{ph}_{hkl} = \frac{d^{ph}_{hkl} - d^{ph,0}_{hkl}}{d^{ph,0}_{hkl}} \tag{2}$$

The particular DEC_{hkl} are evaluated by linear regression of the macroscopic true stress versus the lattice strain. As an upper boundary for the regression, the maximum yield stress at zero plastic strain (YS_0) is used, as introduced in Vitzthum et al. [12]. The lattice plane specific phase stress is calculated by equation (3).

$$\sigma_{hkl}^{ph} = DEC_{hkl} \bullet \varepsilon_{hkl}^{ph} \quad (3)$$

Based on the assumption that the microstructure is homogeneous and considering the phase fractions (f), the phase stresses σ_{hkl}^{ph} can be recombined with equation (4) and should reflect the macroscopic true stress σ [49]. This procedure can be used to validate the evaluation.

$$\sigma = f_{Fe} \bullet \sigma_{hkl}^{Fe} + (1 - f_{Fe}) \bullet \sigma_{hkl}^{Ma} \quad (4)$$

With the measurement methodology used to investigate the material behavior, it is not possible to determine initial interphase stresses or lattice strains that are already introduced due to the manufacturing process of the steel sheets. The results are therefore relative to the initial state and not absolute values.

5. Results

It is noted that the results shown for the cyclic tensile test in Fig. 9 (a–c), 10–17 are one and the same test. Except for the additional information about the IF steel in Fig. 15. For the tension-compression test, Fig. 9 (d–f) and 18–20 are the same test. The results were prepared and presented specifically for the objective of the particular analysis.

Fig. 10 shows the true stress versus lattice strain curves for the lattice planes (200) and (211) in the cyclic tensile test for a better classification of the following analyses in the overall test. As already described, martensite and ferrite are evaluated separately. Since the behavior of the lattice plane (110) was analogue to the one of (211), only (211) is shown here. An important question with respect to micro plasticity models is whether and to what extent the martensitic phase plasticizes [27]. Zecevic et al. [26] showed the importance of this fact for modeling approaches. Lattice strains evaluated on basis of diffraction can only be detected during elastic deformation. Hence, if the lattice plane is plasticized, no more lattice strain can be absorbed [50]. The onset of yielding is indicated by vertical asymptotic behavior in Fig. 10. It can be seen for both lattice planes that the ferrite shows this vertical behavior from around 700 MPa on. After each unloading-loading cycle, it approaches this vertical curve again. Thus, the ferrite clearly plasticizes during the tensile test. The martensite appears to be able to accommodate strain at any point in the test and no clear plasticization is recognizable. Only when the ferrite plasticizes, the slope in the martensite changes and even more strain is absorbed. A closer look at the martensite of the lattice plane (211) reveals that the slope in Fig. 10 (b) changes again at high plastic strains and less elastic lattice strain can be absorbed. This may indicates a slight plasticization of the martensite and experimentally confirms the results in [26], where the assumption of a plastic deformability of the martensite improved the simulation result. Looking at the absolute values of the martensite phase, one can see that the (200) lattice plane is significantly softer than the one on basis of the measurement of the lattice plane (211). The martensite of the (200) lattice plane absorbs around double the strain as the martensite of the lattice plane (211). Hence, the behavior differs greatly between lattice planes and is microscopically highly anisotropic. Whereas the martensite lattice strain steadily increases, the ferrite lattice strain becomes more and more negative during unloading at higher plastic strains. In the following, the microstructural behavior shown in Fig. 10 is described in detail.

5.1. Onset of yielding

Fig. 11 shows the macroscopic true stress versus true strain curve for the in-situ, cyclic tensile test, performed under synchrotron radiation. Marked are the temperature-dependent elasticity parameters yield stress at temperature minimum (YS_{Tmin}) and yield stress at zero plastic strain (YS_0), which are determined according to a previous study [12]. Furthermore, the commonly used equivalent yield strength at 0.2 % plastic strain ($YS_{0.2\%}$) was added. It is remarkable that there are large differences between the three parameters, especially in the first loading. According to Vitzthum et al. [12], YS_0 represents the onset of plastic yielding, investigated for a single-phase steel. This study will now also investigate the temperature-dependent determination method for the dual-phase steel. The YS_0 at 421 MPa is significantly lower than the YS_{Tmin} at 553 MPa and $YS_{0.2\%}$ at 700 MPa. In the following loadings, YS_{Tmin} and YS_0 differ less. This behavior is caused by grain to grain yielding, so differences in the plasticization between the lattice planes [12,44,45]. Once the slip systems are activated, the particular lattice planes behave similarly and the parameters YS_0 and YS_{Tmin} are closer together [12]. This can be seen also for the dual-phase steel in Fig. 11. $YS_{0.2\%}$ is still significantly higher.

The onset of yielding of the dual-phase steel has to be investigated on a micro level to analyze the relation with the thermoelastic effect. Fig. 12 shows the martensite and ferrite lattice planes versus the

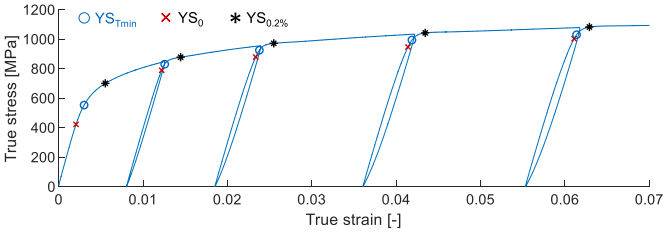

Fig. 11. Macroscopic true stress versus true strain curve for investigated in-situ, cyclic tensile test (DP1000). Temperature-dependent elasticity parameters YS_{Tmin} and YS_0 as well as equivalent yield strength $YS_{0.2\%}$ are marked for every loading cycle.

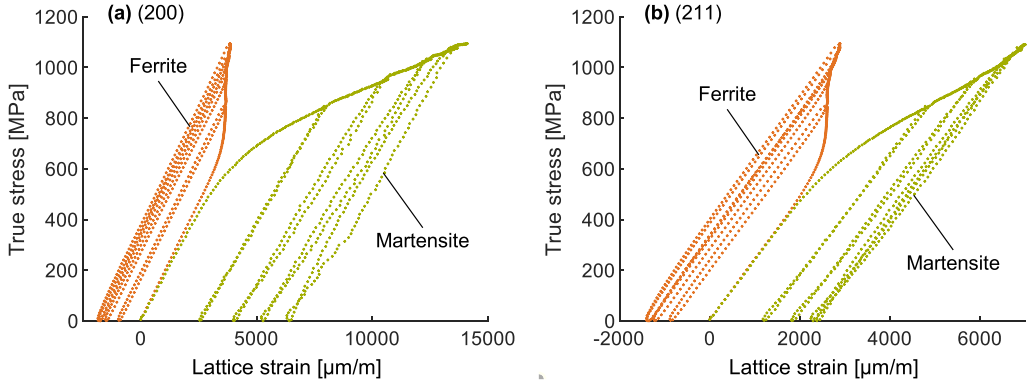

Fig. 10. True macroscopic stress versus lattice strain curves for the lattice planes (200) and (211). Shown are the curve for the ferrite and martensite phases separately. Each point represents a diffraction measurement.

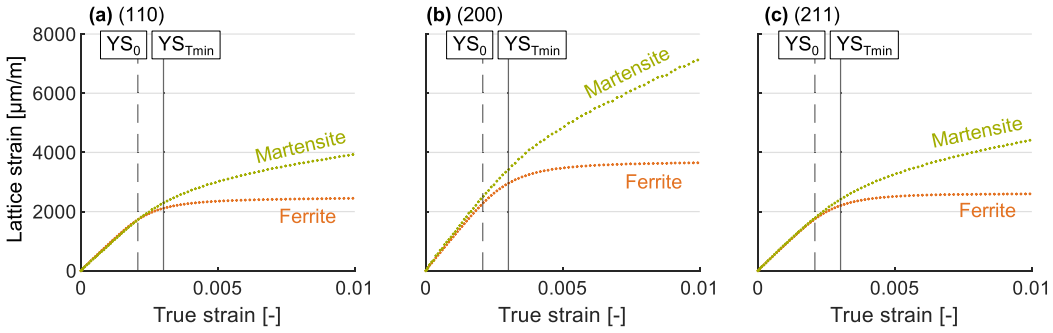

Fig. 12. Lattice strain versus true macroscopic strain for the initial loading for the lattice planes (110), (200) and (211). Marked are the temperature-dependent parameters for the onset of yielding YS_0 and YS_{Tmin}. Each point represents a diffraction measurement.

macroscopic true strain for the initial loading of the material. For all of the considered lattice planes, the lattice strain of the martensite and ferrite increases equally and linearly at the beginning, thus during pure elastic deformation. At a certain point, the ferrite start to leave linearity and converges to a horizontal one, thus, it starts to plasticize. This is the point in time where the behavior between the two phases starts to differ, because the martensitic strain further increases.

Like in [12] shown, the YS_0 parameter again represents the starting point of the elastic-plastic transition of the ferrite, so the onset of plastic yielding. At the point in time of the temperature minimum (YS_{Tmin}) none of the ferrite lattice planes can absorb any more strain. Caused by the plasticization of the ferrite, the martensite further absorbs strain with a different slope. In summary, the two temperature-dependent elasticity parameters YS_0 and YS_{Tmin} again reflect the plastic onset of yielding of the material due to the plasticization of the ferrite.

In order to investigate the early plasticization and the large difference between YS_0 and YS_{Tmin}, the grain to grain yielding effect has to be analyzed. Fig. 13 shows the true stress versus lattice strain curves of the three considered lattice planes for ferrite and martensite. At first glance, the most remarkable characteristic is the strongly different slope of the lattice planes in the initial elastic region for both ferrite and martensite. This indicates a pronounced microstructural anisotropy. Whereas the (211) and (110) lattice plane behave quite identical, the (200) lattice plane shows a more compliant behavior. Tomota et al. [45] investigated a pure ferritic low carbon steel by neutron diffraction. A standard tensile test with measurement stops was performed. The behavior of the lattice strain was also evaluated and it was shown that the lattice plane (200) is the most compliant one. Consequently, despite the second phase, the studied ferrite behaves similarly to the single phase material in [45] and the results are in good agreement. It can be clearly seen that the lattice planes behave distinctly different in their elastic-plastic transition. Looking at the ferrite, the (110) lattice plane starts to deviate from linear behavior first, closely followed by the (211) lattice plane. The (200) lattice plane is still linearly elastic at this point and begins to plasticize later. Again, the parameter YS_0 shows the stress value at which the first lattice planes begin to plasticize, and hence the starting point of grain to grain yielding. It can be seen that from the time of YS_{Tmin} all lattice planes plasticize. Looking at the martensite, no real change in the behavior around YS_0 can be seen. At YS_{Tmin} the slopes change and more lattice strain is absorbed compared to the initial elastic range. It is more likely that this behavior is based on the plasticization of the ferrite phase.

5.2. Elastic loading modulus

In section 5.1, it was confirmed that the parameter YS_0 precisely reflects the onset of plastic yielding for DP steels also. Accordingly, it is reasonable to use this value as an upper limit for determining the loading modulus (E_{YS0}) [12]. Moreover, this value within this work was also used as an upper limit for determining the DEC_{hkl}. Table 3 shows the DEC^{ph}_{hkl} for the lattice planes separately for ferrite and martensite as well as the macroscopic loading modulus E_{YS0} for the initial loading. The (211) and (110) DEC^{ph}_{hkl} hardly differ, and also between martensite and ferrite. With around 240 GPa their value is significantly higher than the macroscopic E_{YS0} with 202 GPa. The macroscopic value is in good agreement with literature and the expected value for steel. As mentioned earlier, the (200) lattice plane is significantly softer and this is reflected in the DEC^{Fe}_{hkl} at 185 GPa. It is noticeable that for the (200) lattice plane, ferrite and martensite differ more clearly with a DEC^{Ma}_{hkl} of 170 MPa for martensite. This can be explained by polycrystalline grain interactions and significant strain anisotropy for the (200) lattice plane, which is why

Table 3
DEC and macroscopic loading modulus E_{YS0} in [GPa] for the initial loading.

DEC_{110}		DEC_{211}		DEC_{200}		E_{YS0}
Fe	Ma	Fe	Ma	Fe	Ma	–
243.3	243.7	240.0	236.1	185.2	170.0	202.0

Fe = Ferrite | Ma = Martensite

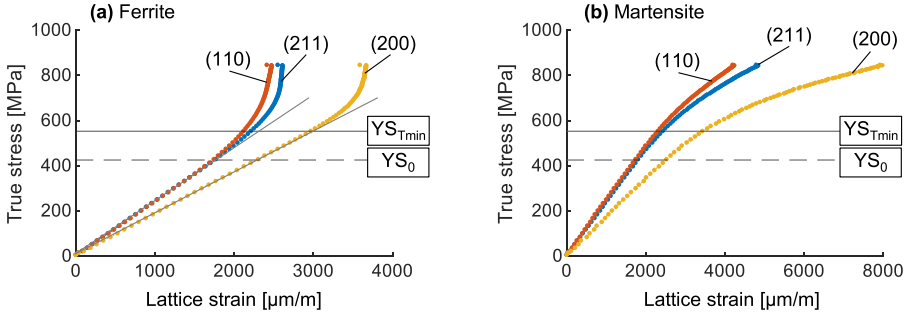

Fig. 13. Comparison of initial onset of yielding of the lattice planes (200), (110) and (211) for (a) ferrite and (b) martensite.

the behavior of the plane is less reliable [34]. Furthermore, the measured intensity for the lattice plane (200) is significantly lower than for the lattice planes (211) and (110). This means that there is a small number of these orientations for the material under investigation. This leads to a greater variation of the results and thus to a comparatively lower accuracy. For this reason, the mentioned difference in the DEC between martensite and ferrite will not be discussed further. Woo et al. [32] recommends the more detailed analysis of the (211) lattice plane, as it is more representative and also the standard lists the (211) lattice plane for bcc material as being less sensitive to intergranular strain [51]. For these reasons, the lattice plane (211) is mainly used to correlate the microscopic with the macroscopic behavior.

Furthermore, the loading moduli E_{YS0} are evaluated with the introduced temperature-dependent determination method for the four following loadings during the cyclic tensile test. Fig. 14 shows the plastic strain-dependent behavior of the macroscopic E_{YS0} in comparison with the diffraction elastic constant of (211) lattice plane for ferrite and martensite. The DEC^{ph}_{hkl} do not change with increasing plastic strain, whereas the E_{YS0} decreases to 180 GPa at 5.5 % plastic strain. So, there is a decrease of around 10 % compared with the initially measured parameter. It is important to note that this is the evaluation of the loading modulus. The chord modulus, i.e. the unloading modulus, decreases even more with increasing plastic deformation. The decrease of the macroscopic modulus must therefore be based on other effects in the microstructure.

5.3. Anelasticity

Before going into more detail at a micro level, the nonlinear or anelastic behavior will be quantified macroscopically. To better clarify the origin of the specific elastic behavior of martensitic-ferritic steels, the anelastic behavior, loading and unloading moduli are compared with a single-phase purely ferritic IF steel (HC260Y), recorded with similar experimental conditions (see Fig. 15). The anelastic strain is determined by equation (1) for the first four unloading-loading cycles (see Fig. 15 (a)). To provide a better comparative value, the anelastic strain (ε_{an}) is given as a percentage of the total springback strain (ε_{sb}). Fig. 15 (a) clearly shows the significantly higher portion of anelastic strain for the DP steel compared with the single-phase steel. The anelastic portion increases especially in the beginning of plastic deformation and seems to converge at higher plastic strains. As already mentioned in the state of the art, there are two plausible explanations for the anelastic behavior. One of them is dislocation motion and the other are interphase stresses. Since the single-phase material exhibits anelastic behavior, however much less than the dual-phase material, is clear that

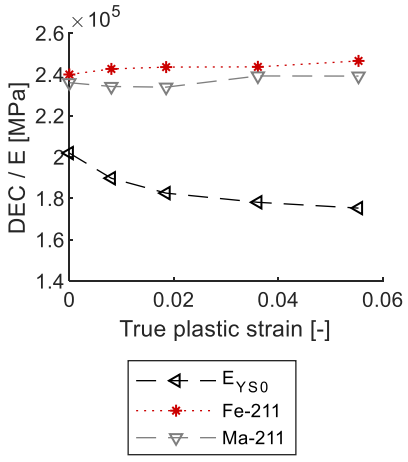

Fig. 14. Plastic strain dependency of loading modulus E_{YS0} in comparison with DEC (211).

none of the effects can be excluded, since no interphase stresses can definitely be present here. Fig. 15 (b) shows the loading (E_{YS0}) and unloading (E_{chord}) moduli for both materials. All moduli decrease with increasing plastic strain and their increase seems to be the inverse to the behavior of the anelastic portion. Here, in the beginning of plastic deformation, the moduli decrease rapidly until they converge with further plastic deformation. Hence, a relation between the anelastic strain and the strain-dependency of the elastic moduli is obvious. Again, the loading and unloading moduli for the single-phase material also decrease with increasing plastic strain, but significantly less than the moduli for DP steel. Furthermore, the differences between E_{YS0} and E_{chord} are higher for DP steel than for IF steel, which indicates higher nonlinearity in the elastic unloading curve.

In-situ diffraction experiments allow a phase specific evaluation and therefore this analysis method is appropriate for the evaluation of phase stresses. Due to the separation between ferrite and martensite reflections, it is possible to determine their phase stresses separately using equation (3). To validate the evaluation, the individual phase stresses are recombined using equation (4) and compared with the experimental macroscopic results. Fig. 16 shows the martensite and ferrite phase stress versus the true macroscopic strain for the lattice plane (211). It can be seen that the martensite absorbs significantly more stress than the ferrite. After plasticization, the latter shows a horizontal behavior, i.e. no further stress can be absorbed. The combined curve in Fig. 16 represents the stress-strain calculated with the volume fractions and phase stresses of martensite and ferrite using equation (4). The curve is in good agreement with the macroscopic experimental true stress versus true strain curve (gray circles). Hence, the determination of the phase fraction by means of SEM and the evaluation of the phase stresses seems to be valid.

The separate evaluation of phase stresses allows the determination of the delta between them and thus the correlation of interphase stresses or residual stresses of 2nd order and the macroscopic anelastic behavior. For better understanding, Fig. 17 (a) again shows the martensite and ferrite phase strain for (211). Now, the particular phase stresses at macroscopically unloaded state (0 MPa) are marked for both phases. The tensile specimen is therefore completely load-free at this point. In Fig. 17 (b), this delta in phase stresses is plotted versus the true plastic strain. It is noticeable that the interphase stresses increase with plastic strain in the same way as the anelastic strain (see Fig. 15 (a)). At the beginning, the interphase stresses increase strongly and then converge with increasing plastic strain. This behavior can be explained by the individual phase stresses. The soft ferrite phase plasticizes much earlier than the martensite at around 600 MPa. From this on, the ferrite cannot absorb any more stress and all the stress has to be absorbed by the harder martensite phase. It can be seen that the phase stress of the martensite increases strongly in the beginning of plastic deformation, hence shows a very high hardening. The phase is still not fully plasticized, and elongates elastically. This discrepancy leads to a compressive state in the ferrite phase. With increasing plastic deformation, also the martensite hardly absorbs any stress, so the delta between the two phases does not change anymore. This behavior, and especially the trend with respect to increasing plastic strain, strongly indicates that the origin of at least part of the anelastic strain lies in the behavior of the phase stresses. In addition, this separate approach to phase stresses in cyclic tensile tests offers potential for micro modeling approaches. Generally, it can be stated that the saturation of the Young's modulus decrease with increasing plastic strain mainly comes from the behavior of the martensite phase.

5.4. Re-yielding

In the literature, the Bauschinger effect is often discussed together with re-yielding [52]. It means that after a load change, the material starts to plasticize again earlier than without a load change. Especially for materials with strong Bauschinger effect like the considered DP1000,

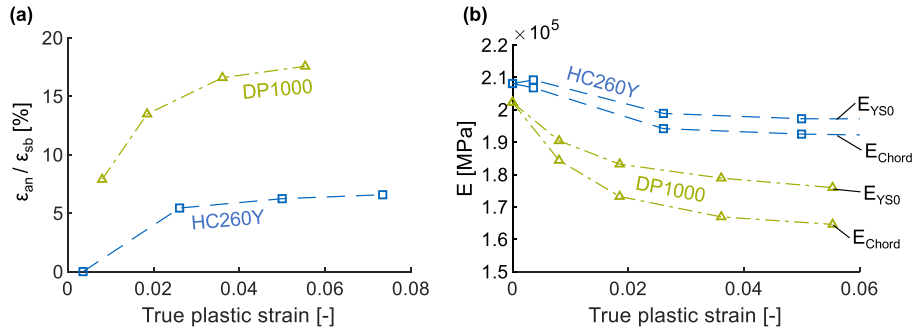

Fig. 15. (a) Anelastic strain relative to the recovery strain for DP1000 and the single-phase IF steel HC260Y; (b) Plastic strain dependency of the E_{YS0} and E_{chord} moduli, also in comparison with the HC260Y steel.

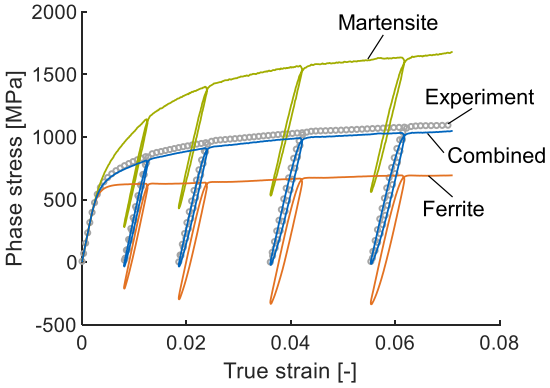

Fig. 16. Martensite and ferrite phase stresses of lattice plane (211). The experiment represents the macroscopic true stress versus true strain curve. The combined curve represents the stress versus strain curve calculated with the phase stresses and volume fractions of martensite and ferrite (see equation (4)).

the re-yielding behavior is crucial for the accuracy of springback prediction [2]. Furthermore, it is discussed, whether for some materials, the re-yielding takes place already in the tension state, so before compression [18]. To investigate this behavior, tension-compression tests are necessary to analyze the micro behavior during unloading and compressive loading. Within this study in-situ tension-compression tests were performed and the macroscopic true stress versus true strain curve can be seen in Fig. 5 (b). The in-situ diffraction and profile analysis were performed analogously to the evaluation of the cyclic tensile test. Fig. 18 shows the martensite and ferrite phase stresses and their combination calculated by equation (4). Again the combined curve is in very good agreement with the experimental macroscopic true stress versus true strain curve (gray circles).

Fig. 19 shows, similar to Fig. 13, the true stress versus relative lattice strain for the lattice planes (110), (200) and (211) divided in ferrite (a) and martensite (b). Only the unloading and subsequent compressive loading are shown. For better comparability, the lattice strains were zeroed at the start of the unloading, so the values are relative. When looking at the ferrite (see Fig. 19 (a)), one notices that the lattice planes again differ significantly in their elastic behavior. Again, the (200) plane shows the softest behavior. It can also be seen that during elastic unloading, i.e. in the tensile region, the lattice strains decrease linearly. A clear plasticization can only be seen in the compression range, where no further elastic lattice strain can be absorbed. But it can be seen that the behavior of the lattice strains changes around the point of zero macroscopic true stress. In the compression range, the behavior is no

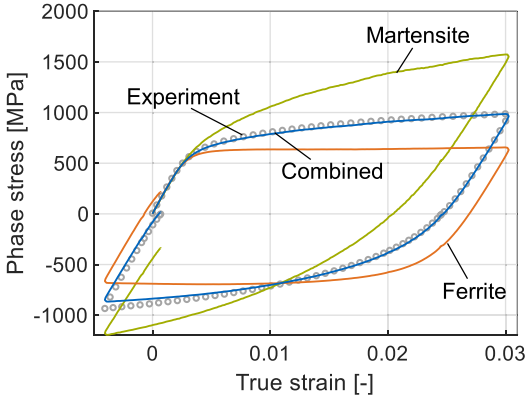

Fig. 18. Martensite and ferrite phase stresses (211) and their combination compared with the experimental macroscopic data.

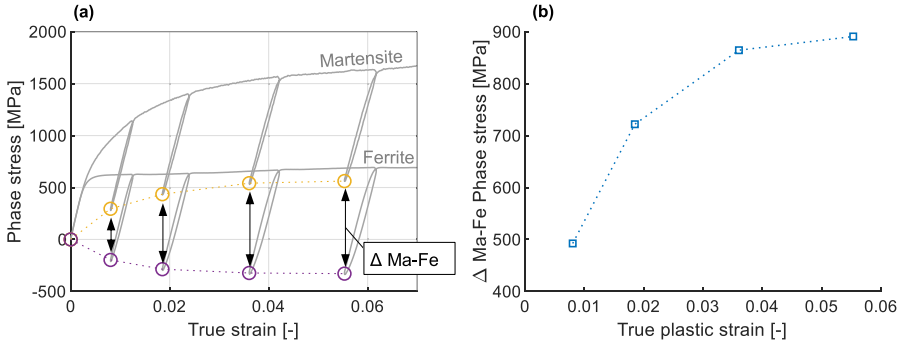

Fig. 17. (a) Comparison of martensite and ferrite phase stress for cyclic tensile test for the lattice plane (211). Marked are the phase stress values at macroscopically unloaded state (0 MPa) and their delta is drawn with arrows. (b) Delta between martensite and ferrite phase stress for macroscopically unloaded state versus true plastic strain.

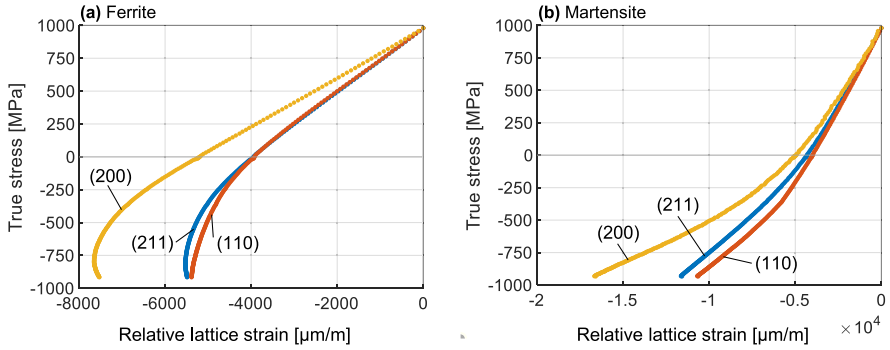

Fig. 19. True stress versus relative lattice strain of the elastic unloading and following compression after 3% true prestrain. Shown are three lattice planes for (a) ferrite and (b) martensite. For better comparability, the lattice strains were zeroed at the start of unloading.

longer linear. This indicates that the planes are already beginning to plasticize. One reason for this different behavior may be a strength difference between tension and compression, i.e. tension and compression asymmetry. To exclude this, initial compression tests were performed with the same test setup and the initial behavior of martensite and ferrite for tension and compression were compared. No significant difference could be detected.

The grain to grain yielding described above is clearly visible. The martensite behaves very differently from the ferrite (see Fig. 19 (b)). While ferrite seems to plasticize around zero stress and in the beginning of the compression range, martensite never reaches a state where elastic lattice strain can no longer be absorbed. The martensite therefore does not plasticize in compression. On closer examination, it is noticeable that the martensite begins to leave the linear behavior under elastic strain even earlier than the ferrite. Already before the zero stress crossing, the curves change to non-linear behavior. Since it is already known from the onset of yielding that the behavior of the martensite changes when the ferrite plasticizes, this is a further indication that a very early plasticization of the ferrite occurs.

In the following, the phase stresses and, in particular, their difference, i.e. the interphase stresses in the tension-compression test, will be discussed in more detail. Fig. 20 (a) again shows the martensite and ferrite phase stresses versus the true strain of the tension-compression test for the lattice plane (211). It is known from the results of the cyclic tensile tests that the interphase stress increases significantly in the beginning of plastic deformation and at the same time the elastic moduli decrease strongly. At state 1 in Fig. 20 (a), the macroscopic stress is zero, so there is an interphase stress of 846 MPa between the martensite and ferrite. Again, the ferrite is already in the compressive state. Compared with the linearly interpolated result of the cyclic tensile test in Fig. 17 (b), this value is about 70 MPa higher. This increased value is explained by the fact that the cyclic tensile test was preceded by an unloading-reloading cycle, which can slightly change the residual stresses present. In addition, the material shows significant microscopic inhomogeneities, so that deviations between specimens are possible with the local measuring method. A difference in the initial state is also conceivable as a reason for the deviation. Fig. 20 (b) shows the true stress versus true strain curve and the result for the chord modulus for the elastic unloading until zero stress after tensile loading. The chord modulus $E_{\mathrm{chord,T}}$ decreased according to the results shown in Fig. 15 (b) to 173.4 GPa. The behavior under tension thus fits very well into the results of the cyclic tensile test (see Fig. 17). After the initial tensile load, the specimen was compressed to - 0.4% strain. The ferrite phase stress reaches a maximum value of 656 MPa shortly in tension just before unloading and a maximum compressive stress of - 695 MPa again shortly before unloading. This shows that roughly the same stress can be absorbed by ferrite in tension and compression. It is assumed that the slightly increased value in compression occurs due to hardening, as dislocations are formed in tension. The martensite phase stress has maximum values of 1573 MPa and - 1194 MPa and thus an absolute delta of 379 MPa. The martensite therefore takes less stress in compression. But, it can also be seen in the macroscopic curve (see Fig. 20 (b)), that the maximum tensile stress is not reached in compression. State 2 in Fig. 20 (a) reflects the final state of the experiment at zero stress. The interphase stress has now reversed. The large elastic strain of the martensite has resulted in tensile stress during unloading from the compressive load in the ferrite phase. If the elastic modulus now depends on the interphase stress, as written above, this change should also lead to such a change in the elastic modulus. Therefore, a compression chord modulus $E_{\mathrm{chord,C}}$ was determined for the elastic compression unloading curve. And indeed, the chord modulus increases again to 191.7 GPa. The relationship between interphase

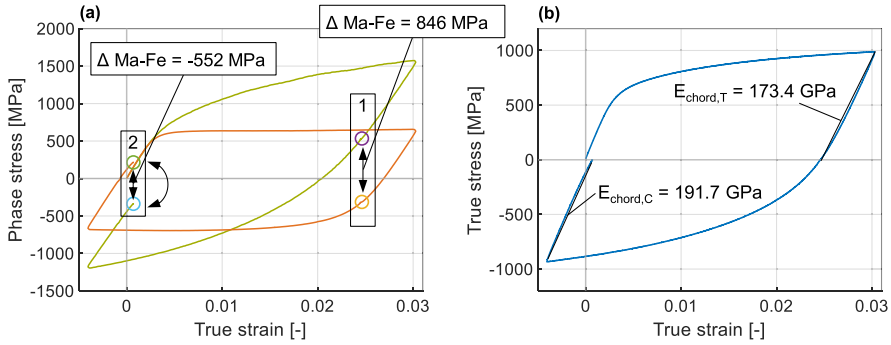

Fig. 20. (a) Martensite and ferrite phase stresses versus true strain for the lattice plane (211) and the tension-compression test. The interphase stresses at zero macroscopic stress after tensile loading (state 1) and after compressive loading (state 2) are plotted. (b) True stress versus true strain curve. Drawn in are the elastic chord moduli for tension ($E_{\mathrm{chord,T}}$) and compression ($E_{\mathrm{chord,C}}$).

stresses and the behavior of the elastic modulus is thus obvious. As already mentioned, two effects, namely dislocation motion and interphase stress, probably influence the elastic behavior of dual-phase steels. The recovery of the elastic modulus shows that the material can recover under compressive loading. It appears that dislocations can be annihilated. This result can be confirmed with the peak profiles in Fig. 9 (d–f). It can be seen that the experimentally measured points corresponding to the sum curve of the two peaks become narrower again and the maximum intensity increases (see Fig. 9 (f)). A decreasing peak width indicates the reduction of lattice defects and thus, can indicate nihilation of dislocations. Again, the influence of considering the nihilation of dislocations, studied numerically in Zecevic et al. [26], can be confirmed experimentally.

6. Conclusions

Within this study, the specifics of the elastic-plastic material behavior of high-strength dual-phase steel were investigated using in-situ diffraction experiments. The elastic onset of yielding, the strain dependence of the elastic modulus, anelastic strain behavior and re-yielding after load change were analyzed by means of cyclic tensile tests and tension-compression experiments under synchrotron radiation. With the evaluation approach of the diffraction profiles it was possible to evaluate ferrite and martensite separately from each other. Thus, interphase stresses could be determined and directly compared to the macroscopic material behavior. The key results of the work can be summarized as follows:

- It was shown that the distinct softer ferrite phase begins to plasticize, affecting the strain behavior of the harder martensite. The martensite phase shows a much greater capacity to absorb elastic strain and direct plasticization did not occur in the considered strain range.
- The onset of yielding was determined on the basis of the thermoelastic effect, which could thus also be qualified microscopically for dual-phase materials. The temperature-dependent determination of the Young's modulus was applicable and provided reasonable results.
- By evaluating the phase stresses, it was shown that the martensite absorbs significantly larger stresses and confines the ferrite phase to compression when the specimen is elastically relieved. The connection of these residual stresses of the 2nd order with the anelastic strain behavior could be established.
- By microstructural evaluation of the tension-compression test, the re-yielding behavior was analyzed and a clear Bauschinger effect could also be demonstrated microscopically. Furthermore, it could be shown that the material can recover during load changes due to the interaction of martensite and ferrite. The phase stresses occurring in this process led to an increase in the macroscopic Young's modulus after compressive loading.

In general, the results of this work provide in-depth material understanding by considering the cyclic tension tests and tension-compression tests, which are crucial for investigating elastic material behavior, through the high microscopic resolution of the in-situ synchrotron diffraction experiments. The study deals with a DP1000 steel, which is of great importance in industrial applications due to its strength-to-weight ratio. This knowledge has great potential to improve material characterization on the one hand and micro plasticity models on the other. In a next step, both the experiment and the evaluation approach have to be further improved and compared with optical methods such as TEM measurements, so that the peak broadening and thus the micro strain or dislocation behavior of the individual phases can be investigated in more detail. In this way, not only the interphase stresses, as in this work, but also the dislocation behavior in terms of anelasticity and Bauschinger effect can be further analyzed and quantified.

CRediT authorship contribution statement

Simon Vitzthum: Conceptualization, Methodology, Investigation, Software, Writing – original draft, Writing – review & editing, Visualization, Formal analysis, Data curation. **Joana Rebelo Kornmeier:** Conceptualization, Methodology, Investigation, Formal analysis, Validation. **Michael Hofmann:** Supervision, Project administration, Conceptualization, Methodology, Formal analysis, Validation. **Maximilian Gruber:** Investigation, Validation. **Roman Norz:** Investigation, Validation. **Emad Maawad:** Investigation. **Joseba Mendiguren:** Investigation, Formal analysis, Validation. **Wolfram Volk:** Supervision, Project administration, Validation, Funding acquisition.

Declaration of competing interest

The authors declare that they have no known competing financial interests or personal relationships that could have appeared to influence the work reported in this paper.

Data availability

The raw/processed data required to reproduce these findings cannot be shared at this time as the data also forms part of an ongoing study.

Acknowledgments

The author would like to thank the German Research Foundation (DFG) for the financial support under the grant number 429432653. Furthermore, the authors would like to thank the team of Hereon Geesthacht for the measurement opportunity at the side station of the HEMS beamline at PETRA III synchrotron (DESY).

References

[1] J. Mendiguren, F. Cortés, X. Gómez, L. Galdos, Elastic behaviour characterisation of TRIP 700 steel by means of loading–unloading tests, Mater. Sci. Eng. 634 (2015) 147–152.
[2] F. Yoshida, T. Amaishi, Model for description of nonlinear unloading-reloading stress-strain response with special reference to plastic-strain dependent chord modulus, Int. J. Plast. 130 (2020), 102708.
[3] R.H. Wagoner, H. Lim, M.-G. Lee, Advanced issues in springback, Int. J. Plast. 45 (2013) 3–20.
[4] D. Li, R.H. Wagoner, The nature of yielding and anelasticity in metals, Acta Mater. 206 (2021), 116625.
[5] R. Hooke, A Description of Helioscopes and Some Other Instruments Made by Robert Hooke, in: Fellow of the Royal Society, Printed by T.R. for John Martyn, 1676.
[6] S. Ledworuski, M. Ell, H.-J. Kühn, Den Elastizitätsmodul sicher bestimmen, Mater. Test. 42 (2000) 109–113.
[7] H.M. Sonne, Bestimmung des Elastizitäsmoduls im Zugversuch, Vortrags- und Diskussionstagung, Bad Nauheim (1999) 219–230.
[8] S. Suttner, M. Merklein, A new approach for the determination of the linear elastic modulus from uniaxial tensile tests of sheet metals, J. Mater. Process. Technol. 241 (2017) 64–72.
[9] G. Sallat, Theoretische und experimentelle Untersuchungen zum Fliessverhalten von Blechen im Zweiachsigen, Dissertation, Chemnitz, 1988.
[10] S. Vitzthum, M. Eder, C. Hartmann, W. Volk, Investigation on strain dependent elastic behavior for accurate springback analysis, J. Phys.: Conf. Ser. 1063 (2018), 12118.
[11] S. Vitzthum, C. Hartmann, M. Eder, W. Volk, Temperature-based determination of the onset of yielding using a new clip-on device for tensile tests, Procedia Manuf. 29 (2019) 490–497.
[12] S. Vitzthum, J. Rebelo Kornmeier, M. Hofmann, M. Gruber, E. Maawad, A. C. Batista, C. Hartmann, et al., In-situ analysis of the thermoelastic effect and its relation to the onset of yielding of low carbon steel, Mater. Des. 162 (2022), 110753.
[13] G.I. Taylor, H. Quinney, The plastic distortion of metals, Philos. Trans. R. Soc. Lond. - Ser. A Contain. Pap. a Math. or Phys. Character 230 (1931) 323–362.
[14] F. Morestin, M. Boivin, On the necessity of taking into account the variation in the Young modulus with plastic strain in elastic-plastic software, Nucl. Eng. Des. (1996) 107–116.
[15] F. Morestin, M. Boivin, C. Silva, Elasto plastic formulation using a kinematic hardening model for springback analysis in sheet metal forming, J. Mater. Process. Technol. (1996) 619–630.
[16] R.M. Cleveland, A.K. Ghosh, Inelastic effects on springback in metals, Int. J. Plast. 18 (2002) 769–785.

[17] L. Luo, A.K. Ghosh, Elastic and inelastic recovery after plastic deformation of DQSK steel sheet, J. Eng. Mater. Technol. 125 (2003) 237.
[18] F. Yoshida, T. Uemori, K. Fujiwara, Elastic–plastic behavior of steel sheets under in-plane cyclic tension–compression at large strain, Int. J. Plast. 18 (2002) 633–659.
[19] F. Yoshida, Description of non-linear unloading curve and closure of cyclic stress-strain loop based on Y-U model, J. Phys.: Conf. Ser. 1063 (2018), 12094.
[20] C. Zener, J.H. Hollomon, Problems in non-elastic deformation of metals, J. Appl. Phys. 17 (1946) 69–82.
[21] C.M. Zener, S. Siegel, Elasticity and anelasticity of metals, J. Phys. Colloid Chem. 53 (1949) 1468.
[22] Z. Arechabaleta, P. van Liempt, J. Sietsma, Quantification of dislocation structures from anelastic deformation behaviour, Acta Mater. 115 (2016) 314–323.
[23] Z. Chen, H.J. Bong, D. Li, R.H. Wagoner, The elastic–plastic transition of metals, Int. J. Plast. 83 (2016) 178–201.
[24] A. Torkabadi, Towards an Accurate Springback Prediction: Experiments and Modeling, Dissertation, Twente, 2018.
[25] A. Govik, R. Rentmeester, L. Nilsson, A study of the unloading behaviour of dual phase steel, Mater. Sci. Eng. 602 (2014) 119–126.
[26] M. Zecevic, Y.P. Korkolis, T. Kuwabara, M. Knezevic, Dual-phase steel sheets under cyclic tension–compression to large strains: experiments and crystal plasticity modeling, J. Mech. Phys. Solid. 96 (2016) 65–87.
[27] Y. Bergström, Y. Granbom, D. Sterkenburg, A dislocation-based theory for the deformation hardening behavior of DP steels: impact of martensite content and ferrite grain size, Journal of Metallurgy 2010 (2010) 1–16.
[28] X.X. Zhang, H. Andrä, S. Harjo, W. Gong, T. Kawasaki, A. Lutz, M. Lahres, Quantifying internal strains, stresses, and dislocation density in additively manufactured AlSi10Mg during loading-unloading-reloading deformation, Mater. Des. 198 (2021), 109339.
[29] X.X. Zhang, A. Lutz, H. Andrä, M. Lahres, W.M. Gan, E. Maawad, C. Emmelmann, Evolution of microscopic strains, stresses, and dislocation density during in-situ tensile loading of additively manufactured AlSi10Mg alloy, Int. J. Plast. 139 (2021), 102946.
[30] J. Macchi, S. Gaudez, G. Geandier, J. Teixeira, S. Denis, F. Bonnet, S.Y.P. Allain, Dislocation densities in a low-carbon steel during martensite transformation determined by in situ high energy X-Ray diffraction, Mater. Sci. Eng. 800 (2021), 140249.
[31] Z. Jiang, Z. Guan, J. Lian, Effects of microstructural variables on the deformation behaviour of dual-phase steel, Mater. Sci. Eng. 190 (1995) 55–64.
[32] W. Woo, V.T. Em, E.-Y. Kim, S.H. Han, Y.S. Han, S.-H. Choi, Stress–strain relationship between ferrite and martensite in a dual-phase steel studied by in situ neutron diffraction and crystal plasticity theories, Acta Mater. 60 (2012) 6972–6981.
[33] C. Song, H. Yu, J. Lu, T. Zhou, S. Yang, Stress partitioning among ferrite, martensite and retained austenite of a TRIP-assisted multiphase steel: an in-situ high-energy X-ray diffraction study, Mater. Sci. Eng. 726 (2018) 1–9.
[34] Z.H. Cong, N. Jia, X. Sun, Y. Ren, J. Almer, Y.D. Wang, Stress and strain partitioning of ferrite and martensite during deformation, Metall. Mater. Trans. 40 (2009) 1383–1387.
[35] kloeckner metals, DP Steel, Why is dual phase steel important to autos?. www.kloecknermetals.com/blog/dp-steel-why-is-dual-phase-steel-important-to-autos/.
[36] W. Liu, J. Lian, N. Aravas, S. Münstermann, A strategy for synthetic microstructure generation and crystal plasticity parameter calibration of fine-grain-structured dual-phase steel, Int. J. Plast. 126 (2020), 102614.
[37] e.V. Deutsches Institut für Normung, Prüfung Metallischer Werkstoffe - Zugproben, 50125th ed., Beuth Verlag GmbH, Berlin, 2009.
[38] A.P. Hammersley, FIT2D: An Introduction and Overview, ESRF Internal Report, 1997.
[39] M. Hoelzel, W.M. Gan, M. Hofmann, C. Randau, G. Seidl, P. Jüttner, W. W. Schmahl, Rotatable multifunctional load frames for neutron diffractometers at FRM II—design, specifications and applications, Nucl. Instrum. Methods Phys. Res. Sect. A Accel. Spectrom. Detect. Assoc. Equip. 711 (2013) 101–105.
[40] T. Kuwabara, Y. Kumano, J. Ziegelheim, I. Kurosaki, Tension–compression asymmetry of phosphor bronze for electronic parts and its effect on bending behavior, Int. J. Plast. 25 (2009) 1759–1776.
[41] S. Popović, Quantitative phase Analysis by X-ray diffraction—doping methods and applications, Crystals 10 (2020) 27.
[42] F. Bachmann, R. Hielscher, H. Schaeben, Texture Analysis with MTEX – Free and Open Source Software Toolbox vol. 160, SSP, 2010, pp. 63–68.
[43] Giovanni Esteves, Klarissa Ramos, Chris M. Fancher, Jacob L. Jones, LIPRAS: Line-Profile Analysis Software, North Carolina State University, 2017.
[44] N. Jia, Z.H. Cong, X. Sun, S. Cheng, Z.H. Nie, Y. Ren, P.K. Liaw, et al., An in situ high-energy X-ray diffraction study of micromechanical behavior of multiple phases in advanced high-strength steels, Acta Mater. 57 (2009) 3965–3977.
[45] Y. Tomota, P. Lukas, S. Harjo, J.-H. Park, N. Tsuchida, D. Neov, In situ neutron diffraction study of IF and ultra low carbon steels upon tensile deformation, Acta Mater. 51 (2003) 819–830.
[46] W.H. Bragg, W.L. Bragg, The reflection of X-rays by crystals, Proc. Royal Soc. A: Math. Phys. Eng. Sci. 88 (1913) 428–438.
[47] A.P. Stebner, D.W. Brown, L.C. Brinson, Young's modulus evolution and texture-based elastic–inelastic strain partitioning during large uniaxial deformations of monoclinic nickel–titanium, Acta Mater. 61 (2013) 1944–1956.
[48] Z.Y. Zhong, H.-G. Brokmeier, W.M. Gan, E. Maawad, B. Schwebke, N. Schell, Dislocation density evolution of AA 7020-T6 investigated by in-situ synchrotron diffraction under tensile load, Mater. Char. 108 (2015) 124–131.
[49] E. Gadalińska, A. Baczmański, S. Wroński, L. Le Joncour, C. Braham, M. François, B. Panicaud, et al., Direct determination of phase stress evolution in duplex steel using synchrotron diffraction, Mater. Sci. Eng. 801 (2021), 140355.
[50] Y. Zhao, J. Zhang, Microstrain and grain-size analysis from diffraction peak width and graphical derivation of high-pressure thermomechanics, J. Appl. Crystallogr. 41 (2008) 1095–1108.
[51] Deutsches Institut für Normung e. V., Zerstörungsfreie Prüfung – Standardprüfverfahren zur Bestimmung von Eigenspannungen durch Neutronenbeugung, Beuth Verlag GmbH, Berlin, 2021 (ISO 21432:2019): Deutsche Fassung EN ISO 21432:2020(DIN EN ISO 21432).
[52] M. Kim, J. Ha, J. McNally, Y.P. Korkolis, Transient hardening and R-value behavior in two-step tension and loading reversal for DP980 sheet, IOP Conf. Ser. Mater. Sci. Eng. 1238 (2022), 12002.